SCIENTIFIC REPORTS

OPEN

Highly Crystalline CVD-grown Multilayer $MoSe_2$ Thin Film Transistor for Fast Photodetector

Received: 21 May 2015
Accepted: 15 September 2015
Published: 19 October 2015

Chulseung Jung[1,*], Seung Min Kim[2,*], Hyunseong Moon[1,*], Gyuchull Han[3], Junyeon Kwon[1], Young Ki Hong[1], Inturu Omkaram[1], Youngki Yoon[3], Sunkook Kim[1] & Jozeph Park[1]

Hexagonal molybdenum diselenide ($MoSe_2$) multilayers were grown by chemical vapor deposition (CVD). A relatively high pressure (>760 Torr) was used during the CVD growth to achieve multilayers by creating multiple nuclei based on the two-dimensional crystal growth model. Our CVD-grown multilayer $MoSe_2$ thin-film transistors (TFTs) show p-type-dominant ambipolar behaviors, which are attributed to the formation of Se vacancies generated at the decomposition temperature (650 °C) after the CVD growth for 10 min. Our $MoSe_2$ TFT with a reasonably high field-effect mobility (10 $cm^2/V \cdot s$) exhibits a high photoresponsivity (93.7 A/W) and a fast photoresponse time ($\tau_{rise} \sim 0.4$ s) under the illumination of light, which demonstrates the practical feasibility of multilayer $MoSe_2$ TFTs for photodetector applications.

Smart interface that can provide communication between human beings and digital devices is of great importance in the present and future electronic applications, and intensive research is being carried out in the field of interactive sensing. The latter involves the use of various types of sensors, such as phototransistors that become activated in the presence of light. For instance, active matrix devices consist of at least a driving transistor and switching transistor to afford selective pixel addressing, and active matrix devices incorporating photosensitive thin-film transistors (TFTs) enable the realization of flat panel displays in which specific pixels are locally activated by incident photons[1]. In this regards, smart interface calls for novel active-channel materials to realize high-speed driving transistors and highly sensitive photodetectors.

Layered semiconductors based on transition metal dichalcogenides (TMDs: MX_2 = Mo, W; X = S, Se, Te) exhibit desirable device characteristics, including high mobility (>100 $cm^2 V^{-1} s^{-1}$) and large photoresponsivity (~500 A/W)[2–5], and mechanical flexibility, which make them attractive for active elements in future interactive electronics. Recently, a significant progress has been made in the synthesis of two-dimensional (2D) semiconductors such as single-layer molybdenum disulfide (MoS_2) for electronic and optoelectronic applications, which demonstrated high field-effect mobility (>100 $cm^2/V \cdot s$) and large photoresponsivity (~500 A/W)[2–5], making it attractive for phototransistors. However, the growth of single layers is not favorable for the fabrication of large-area flat panels since it cannot provide sufficient coverage over several square meters under current technologies. In light of this, multilayered structures with high carrier mobility and high photosensitivity are required for the practical large-area sensing applications.

However, indirect-bandgap MoS_2 multilayers exhibit relatively low photoresponse in TFTs[6], unlike direct-bandgap MoS_2 monolayers, although they can provide high field-effect mobility (>100 $cm^2 V^{-1} s^{-1}$) and small subthreshold swing (~70 mV/decade)[7,8]. An advanced local-gate device structure was introduced

[1]Multi-Functional Nano/Bio Electronics Lab., Kyung Hee University, Gyeonggi, 446-701, Republic of Korea. [2]Carbon Convergence Materials Research Center, Korea Institute of Science and Technology, Wanju-gun 565-905, Republic of Korea. [3]Department of Electrical and Computer Engineering & Waterloo Institute for Nanotechnology (WIN), University of Waterloo, Waterloo, ON, N2L 3G1, Canada. *These authors contributed equally to this work. Correspondence and requests for materials should be addressed to S.K. (email: kimskcnt@gmail.com) or J.P. (email: jozeph.park@gmail.com)

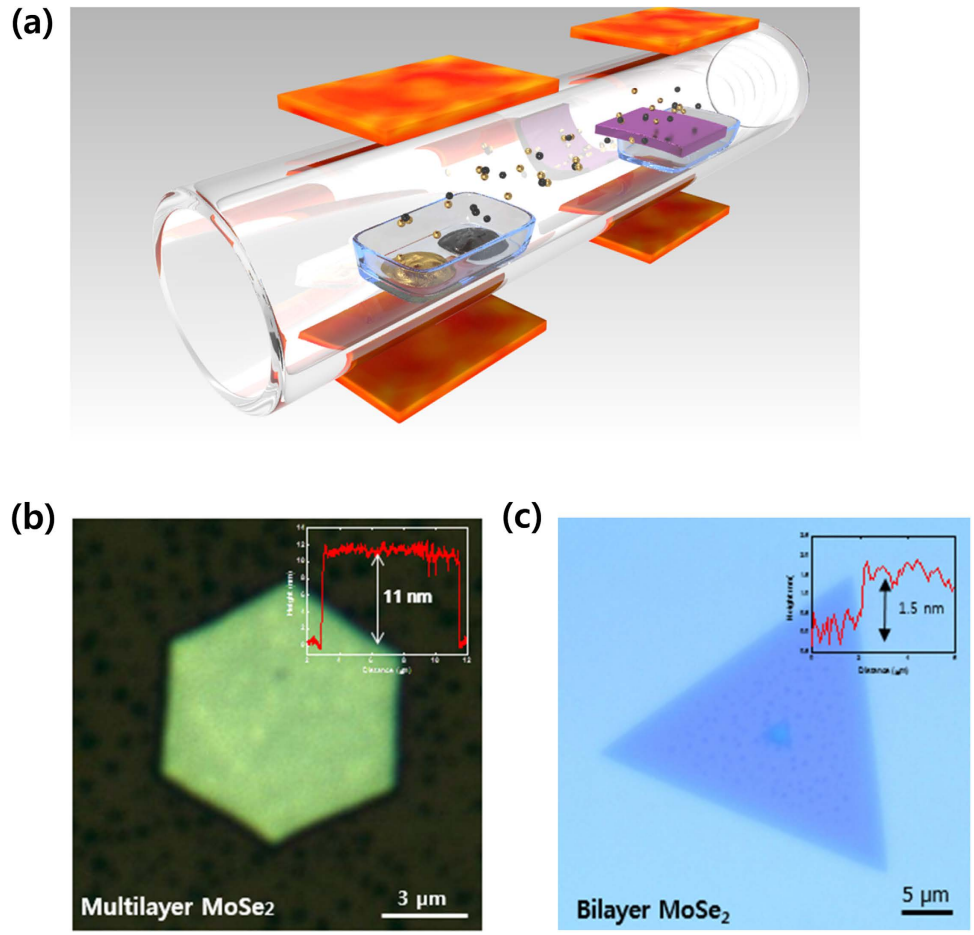

Figure 1. Synthesis of the hexagonal multilayer $MoSe_2$ nanoparticles. (**a**) Schematic process for the synthesis of the hexagonal multilayer $MoSe_2$ nanoparticles with MoO_3 and Se sources. (**b**) Optical microscope images of the as-grown $MoSe_2$ multilayers and (**c**) as-grown $MoSe_2$ bilayer on SiO_2/Si. The insets show the AFM height profile of the as-grown $MoSe_2$ multilayer and bilayer to measure the thickness.

by Kwon *et al.*[9] to enhance the photoresponsivity of multilayer MoS_2 phototransistors. On the other hand, it is known that $MoSe_2$ can provide higher photoresponsivity compared to MoS_2 due to the quantum confinement effect during the bandgap transition[10], which implies that using an advanced device structure may not be needed for $MoSe_2$ phototransistors to achieve high sensitivity. In addition, Choi *et al.*[6] reported that TMD multilayers have an advantage over the monolayers that photoresponse is achievable over a broad range of the electromagnetic spectrum from ultraviolet to near infrared. Therefore, multilayer $MoSe_2$ can be a strong contender for an active channel material of future phototransistors.

In this study, we present the chemical vapor deposition (CVD) growth of $MoSe_2$ multilayers at a relatively high pressure. The CVD methods reported up to date involve low-pressure deposition with slow nucleation rates[11–15], resulting in triangular single layers terminated by either transition metal (*e.g.*, Mo) or chalcogen atom (*e.g.*, Se) for TMDs. In contrast, we demonstrate that indirect-bandgap $MoSe_2$ multilayers can be grown by using a high-pressure CVD method. Based on the two-dimensional nucleation theory, a relatively high pressure at a fixed temperature can induce a large nucleation rate before film growth occurs, and thus, the formation of multilayers is promoted. The microstructure of hexagonal $MoSe_2$ grains is examined using X-ray diffraction (XRD), high-resolution transmission electron microscopy (TEM) and Raman spectroscopy. Our multilayer $MoSe_2$ TFTs exhibit ambipolar behaviors with high photoresponsivity (93.7 A/W) and reasonably large field-effect mobility (~10 $cm^2/V \cdot s$). This highly crystalline and photo-responsive multilayer $MoSe_2$ is anticipated to be used in a myriad of potential applications for interactive electronics.

Results and Discussion

Figure 1(a) shows a schematic CVD process for the growth of hexagonal multilayer $MoSe_2$. Unlike recent studies[16,17], MoO_3 and Se are contained in the same alumina boat located at the upper stream of the CVD furnace. A SiO_2/Si substrate is placed downstream, facing up on the alumina boat and is left to react with the source materials. The furnace temperature was ramped up to 800 °C and 750 °C for the sources and

the substrate, respectively, at a rate of 15 °C/min in an evacuated ambient. The vaporized source molecules are efficiently transferred to the substrate surface by the temperature gradient with the aid of carrier gases such as Ar and H_2. During the chemical reaction between MoO_3 and Se, H_2 gas acts as a catalyst[18]. After the CVD process, hexagonal $MoSe_2$ crystallites of various thickness and size were obtained. Figure 1(b) shows an optical image of an as-grown hexagonal $MoSe_2$ grain with a thickness of approximately 11 nm, measured by atomic force microscopy (AFM). In comparison, Fig. 1(c) shows the height profile of an as-grown $MoSe_2$ bilayer using a relatively low pressure (<760 torr). While the thickness of a $MoSe_2$ monolayer lies generally between 0.6 nm and 1 nm[18–20], hexagonal $MoSe_2$ multilayers obtained in the present work show an average thickness of approximately 12 nm with the size in the range of 4–9 μm. The shape of film depends on the film thickness, which is attributed to the difference in the edge formation energy between Mo-edge or Se-edge termination. In single or few layered $MoSe_2$ films, the difference in the edge formation energy depending on Mo-edge (100) or Se-edge $(\bar{1}00)$ termination results in triangular shaped grains, but since the effect of specific edge termination is cancelled out by alternating Mo- and S-edges in multilayer $MoSe_2$ films, forming a hexagonal shape is expected from the hexagonal crystal structure of $MoSe_2$ film[21].

The relatively large flow rates of injected Ar and H_2 gases in this work are anticipated to increase the pressure in the chamber. Based on two-dimensional nucleation theory[22], a relatively high pressure induces large nucleation rates, and thus multiple nuclei may form on already existing ones, resulting in multilayered structures. The rate of forming stable two dimensional nuclei is usually described by the following equation:

$$Rate = n_s \cdot n^* \cdot \nu \exp\left(-\frac{\Delta G_m}{kT}\right)\exp\left(-\frac{\Delta G_{2D}}{kT}\right) \quad (1)$$

where n_s is the concentration of single adsorbed atoms on a closed packed surface, n^* is the concentration of atoms in contact with a two-dimensional nucleus with a critical size, ν the vibration frequency, ΔG_m the free energy of activation for a surface diffusion jump, and ΔG_{2D} the free energy of formation of a critical nucleus. The latter is again represented by the following relationship:

$$\Delta G_{2D} = \frac{\pi V_m \sigma_s^2(T)}{h \cdot \Delta g} \quad (2)$$

where V_m is the molar volume of the solid phase, $\sigma_s(T)$ is the free energy of step formation per unit length, h the height of the monolayer step, and Δg the difference of molar free energy between the vapor and solid phases in the case of CVD deposition. The growth of $MoSe_2$ layers is attributed to the condensation of vaporized MoO_3 and Se radicals on the substrate, forming Mo_xSe_{2-x} nuclei. As the pressure increases, the n_s also increases, resulting in the enhancement of the nucleation. Another effect of higher pressure is the increase of Δg, as more $MoSe_2$ molecules assemble on the substrate surface. A relatively large Δg value results in decreased ΔG_{2D} barrier, thereby contributing to higher nucleation rate rather than growing from the existing nuclei. It is thus expected that the growth of multilayers is attributed to the formation of additional nuclei to the existing ones with a large nucleation rate. In order to confirm this theory, relatively thin few-layered $MoSe_2$ films were grown at a lower pressure. Figure 1(c) is an optical image of a 1.5 nm-thick $MoSe_2$ grain, which was synthesized at a reduced pressure using lower gas flow rates (Ar: 50 sccm, H_2: 10 sccm). The pressure-dependent film thickness was also demonstrated previously for graphene and graphite layers: Graphite was obtained at relatively high pressures[23], while lower pressures were used for the formation of graphene[24].

Figure 2(a) shows the XRD pattern of our $MoSe_2$ having a clear hexagonal monocrystalline structure[25]. The symmetry of 2H $MoSe_2$ belongs to the space group D^4_{64} ($P6_3/mmc$), which reveals characteristic peaks at $2\theta = 13.72°$, 27.62°, 41.88°, 56.59° and 56.97° corresponding to the (002), (004), (006), (110) and (008) diffractions for $MoSe_2$, respectively. The most intense (002) peak indicates the preferential growth of the $MoSe_2$ crystallites in the (002) direction. To assess the presence and quality of the $MoSe_2$ films, Raman spectroscopy with a laser wavelength of 514.5 nm was carried out. The as-grown $MoSe_2$ atomic layers in this study exhibit several signatures of $MoSe_2$ in the Raman shift ranging from 200 cm^{-1} to 360 cm^{-1}. Along with the out-of-plane A_{1g} mode (Fig. 2(b)) the atomic vibrations corresponding to several less prominent modes including the $E_{2g}{}^1$ (in-plane) and $B_{2g}{}^1$ modes are in agreement with information provided in former reports available in the literature[10,26,27]. The latter modes have significantly lower intensities compared to the most intense out-of-plane A_{1g} peak located at 240.9 cm^{-1}. The typical Raman active modes, *i.e.* the broad & weak $E_{2g}{}^1$ peak located at 287.4 cm^{-1} and the $B_{2g}{}^1$ peak located at 350 cm^{-1}, are observed. The $B_{2g}{}^1$ mode is a shear mode corresponding to the vibration of two rigid layers against each other and appears at relatively low frequencies. The A_{1g} mode is an out-of-plane vibration involving only the chalcogen atoms (Se) while the $E_{2g}{}^1$ mode involves the in-plane displacement of the transition metal (Mo) and chalcogen atoms (Se). Figure 2(c) shows a plan view low magnification TEM image of an as-synthesized $MoSe_2$ flake about 3–4 μm large. The inset in Fig. 2(c) represents a selected area electron diffraction (SAED) pattern taken from within the flake. The pattern reflects well the hexagonal monocrystalline structure along the (002) zone, confirming the XRD results. Figure 2(d) consists of

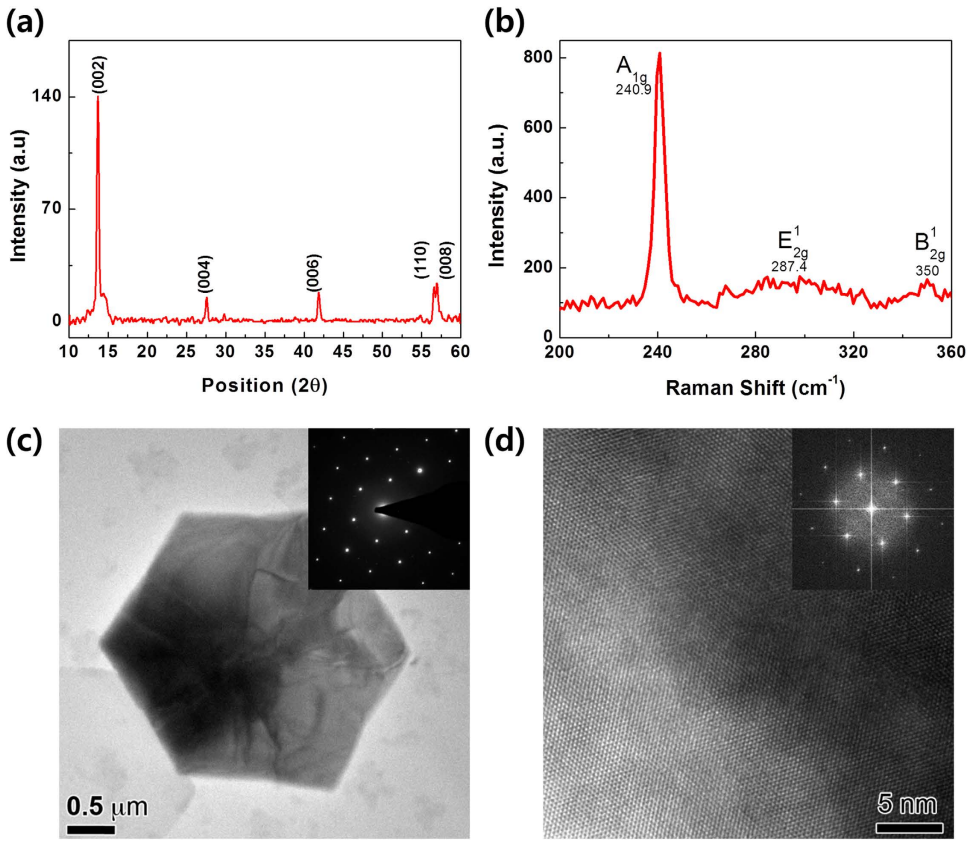

Figure 2. Spectroscopic analyses of CVD-synthesized hexagonal $MoSe_2$. (**a**) XRD pattern of $MoSe_2$ layers indicating the preferential growth in the (002) direction with intense (002), (004), (006), and (008) peaks, along with the presence of a weak (110) peak. (**b**) Raman spectra of $MoSe_2$ with in-plane (E^1_{2g}) and out-of-plane (A_{1g}) vibration modes. (**c**) Plan-view low magnification and (**d**) high resolution TEM images of an as-synthesized $MoSe_2$ flake. The inset in (**c**) is a SAED pattern form within the flake and the inset in (**d**) is a FFT pattern from the entire area of (**d**).

a high resolution TEM image of the thin edge of a $MoSe_2$ flake, and the inset is a fast Fourier transform (FFT) pattern from the entire area of the figure. The above analyses clearly indicate the presence of a highly crystalline hexagonal $MoSe_2$ phase.

Figure 3(a) shows a three-dimensional (3D) schematic of a $MoSe_2$ TFT device. The electrodes consist of Ti as an adhesion layer and Au, and the devices were annealed at 200 °C under atmospheric conditions with Ar and H_2 in order to reduce contact resistance and remove the photoresist remnants. Figure 3(b) shows a 3D topography AFM image, where the thickness of the $MoSe_2$ channel is approximately 20 nm. Figure 3(c) shows the typical drain current (I_{ds}) versus gate voltage (V_{gs}) characteristics of the TFT and the extracted mobility values are also plotted as a function of V_{gs}. The field effect mobility (μ_{eff}) was calculated using the following relationship; $\mu_{eff} = g_m * L/(WC_{ox}V_{ds})$, where L is the channel length (~6.35 μm), W is the channel width (~2.12 μm), C_{ox} is the capacitance of the gate insulator per unit area, and V_{ds} the applied drain-source voltage (1 V). The maximum transconductance, g_m, was extracted to be approximately 54 μS. The devices exhibit an ambipolar behavior with a predominant p-type characteristic, with the highest μ_{eff} being approximately 10 $cm^2/V \cdot s$ and an ON/OFF current ratio of ~10^3, while the electron mobility was extracted as 2.14 $cm^2/V \cdot s$, at the positive region. The output characteristics ($I_{ds} - V_{ds}$) were measured in the negative V_{ds} range (Fig. 3(d)), which also depict clear p-type behaviors.

It is worth investigating the characteristics of p-type $MoSe_2$ TFTs, since most recent studies on $MoSe_2$ TFTs exhibited n-type behaviors[25,28]. Here, it is hypothesized that the band structure of hexagonal $MoSe_2$ multilayers is influenced by a large density of trap sites created by an annealing process during the CVD growth. A recent study demonstrated that irradiation with MeV α particles or thermal annealing at sub-decomposition temperature (~600 °C) creates anion vacancies in TMD materials such as MoS_2, $MoSe_2$, and WSe_2 [29]. Similarly, we can expect that Se vacancies may be created in the present $MoSe_2$ film when the decomposition temperature (~650 °C) is reached after the CVD growth for 10 min. Such defects may also significantly affect the electrical behavior through Fermi level pinning, making the theoretical prediction of the Schottky barrier height ($\Phi_{Bn} = \Phi_m - \chi$, where Φ_m and χ are the metal work function and the semiconductor's electron affinity, respectively) ineffective[30,31]. In order to extract the sub-gap states, a

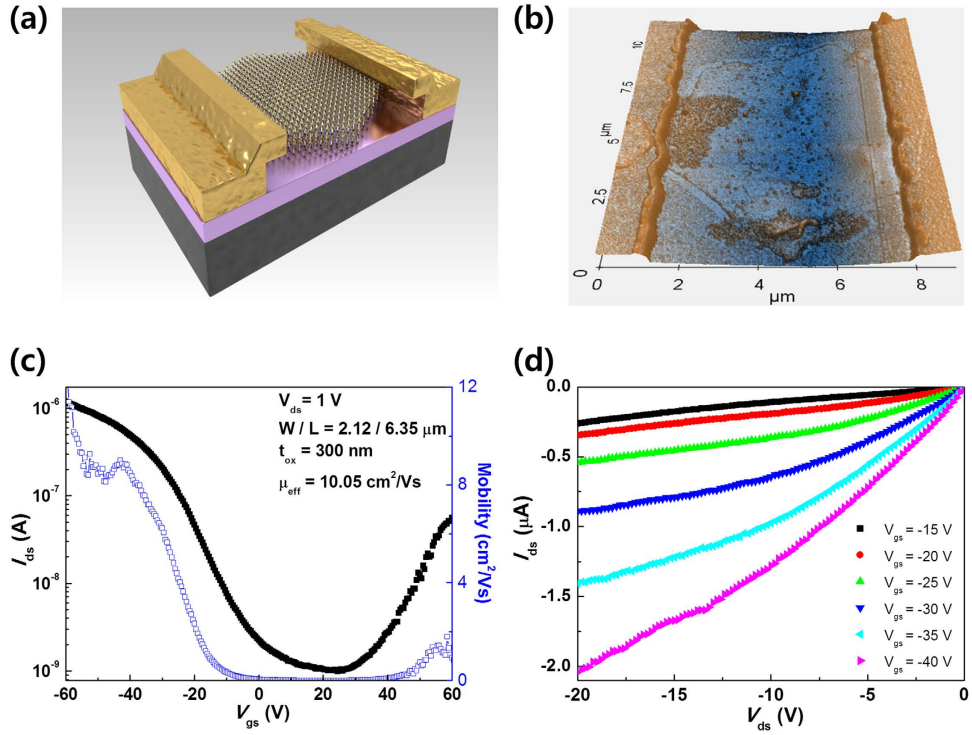

Figure 3. Thin-film transistor based on the CVD-synthesized hexagonal $MoSe_2$ multilayer. (**a**) 3D schematic structure for TFT based on hexagonal multilayer $MoSe_2$ film. (**b**) 3D topography AFM image of the hexagonal $MoSe_2$ TFT with a channel length of 6.35 μm. (**c**) Transfer ($I_{ds} - V_{gs}$) curve and field-effect mobility (μ_{eff}) of the hexagonal $MoSe_2$ TFT ($-60 \leq V_{gs} \leq 60$ V at $V_{ds} = 1$ V). (**d**) Output characteristics of the respective device ($-20 \leq V_{ds} \leq 0$ V, $-15 \leq V_{gs} \leq -40$ V in steps of -5 V).

temperature-dependent analysis was performed[32,33]. Figure 4(a) shows the $I_{ds} - V_{gs}$ characteristics at different temperatures between $T = 300$ and 400 K. Figure 4(b) depicts the thermally activated current at different V_{gs} values, as a function of $1/k_BT$ (where k_B is the Boltzmann constant). The Arrhenius equation is used to describe the current response to the temperature as $I_{ds} = I_{ds,0} \exp\left(-\frac{E_a}{k_BT}\right)$, where $I_{ds,0}$ is a prefactor and E_a is the activation energy[32]. The variation of E_a at different gate voltages is shown Fig. 4(c), from which the density of sub-gap states can be obtained by $N(E) = \frac{C_{ox}}{q}\left(\frac{\partial E_a}{\partial V_{gs}}\right)^{-1}$ where q is the elementary charge. Figure 4(d) shows a large density of sub-gap states in the band gap near $E_V + 0.35$ eV (E_V being the valence band maximum), which is 0.07–0.2 eV below the midgap energy (E_m), since the band gap of bulk $MoSe_2$ is reported to be 0.84–1.1 eV[10,34,35]. Therefore, at the Ti/Au metal–$MoSe_2$ junction, Fermi level pinning[36] caused by the gap states is expected to occur in such a way that the Schottky barrier height for holes becomes smaller ($\Phi_{Bp} \approx E_g/2 - 0.14$ eV) than that for electrons ($\Phi_{Bn} \approx E_g/2 + 0.14$ eV), resulting in p-type-dominant ambipolar behavior as shown in Fig. 3(c).

In order to investigate the optoelectronic properties of $MoSe_2$ multilayers, the photoresponse of the TFTs were examined. Figure 5(a) shows the transfer characteristics under illumination with a 638-nm laser as a function of V_{gs} at various incident power densities (from 20 to 2560 mW/cm^2). The drain bias (V_{ds}) was fixed at 1 V. The photoresponsivity is defined as $R = I_{ph}/(P_{inc}S)$, where R is the photoresponsivity, I_{ph} ($= I_{total} - I_{dark}$) is the photo-induced photocurrent, S is the channel area of the device and P_{inc} (W/cm^2) $= P_{tot}/A_{laser}$ (A_{laser} is the area of laser spot) is the incident power density. The calculated photoresponsivity values with respect to the incident power density are shown in Fig. 5(b). The maximum photoresponsivity of 93.7 A/W was achieved at $V_{gs} = -65$ V with the lowest incident power density (20 mW/cm^2). Notably, this is the highest value reported up to date concerning CVD-grown $MoSe_2$ TFTs, and the photoresponsivity is also comparable to that of mechanically exfoliated $MoSe_2$ TFT[37–40]. Recently, Tongay *et al.*[29] reported that the trap sites related to the anion vacancies, whose energy levels are located between the conduction band (CB) and the valence band (VB), can enhance the photoresponsive properties of TMD. Our temperature-dependent measurements (Fig. 4) also exhibit a large density of sub-gap states in as-grown multilayer $MoSe_2$, which can be the origin of the large photoresponsivity in our multilayer $MoSe_2$ TFTs, by providing excess photo-induced hole carriers upon exposure to light. To evaluate the devices for potential application as photodetectors, the photoswitching behavior was also examined. Figure 5(c) shows the time-resolved drain current when the incident laser is switched on and off with

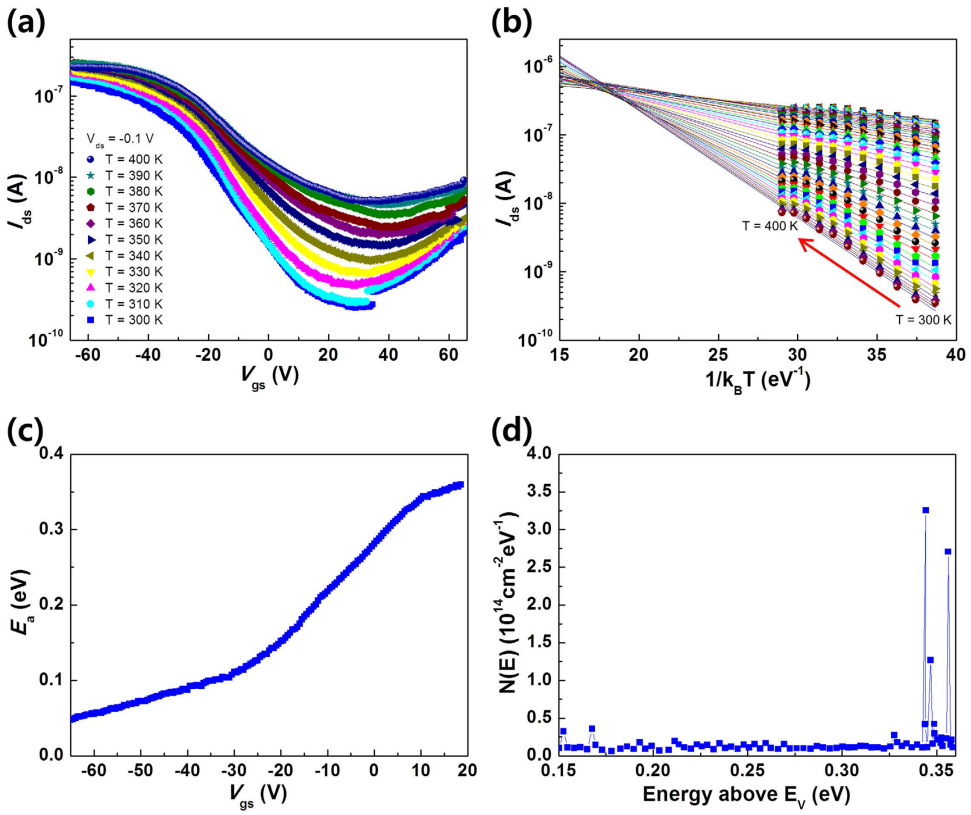

Figure 4. Temperature-dependent behavior and density-of-state measurement according to the Meyer-Neldel rule. (**a**) Transfer characteristics with temperatures from 300 to 400 K in steps of 10 K at $V_{ds} = 0.1$ V. (**b**) Temperature dependence of the drain current (I_{ds}) as a function of $1/k_BT$. (**c**) Activation energy (E_a) extracted using the Meyer-Neldel rule as a function of gate voltage. (**d**) Density of sub-gap states calculated for the p-type $MoSe_2$ TFT as a function of energy above the valence band (E_V). A large density can be observed ~0.35 eV above E_V.

a power density of 2560 mW/cm^2 and a time period of 20 s, while the gate voltage is fixed at 20 V. As shown in Fig. 5(d), the photoswitching behavior consists of a relatively short rising time ($\tau_{rise} \sim 0.4$ s) and a short decay time ($\tau_{decay} \sim 0.2$ s) that form a nearly-ideal rectangular pulse. Such characteristics indicate that $MoSe_2$ devices are promising for photodetector applications.

In conclusion, we presented highly sensitive phototransistors based on CVD-grown hexagonal $MoSe_2$ multilayers. A relatively high pressure (>760 Torr) in the CVD chamber, originating from a large flow rate of injected Ar and H_2 gases, stimulates the formation of multiple nuclei, resulting in multilayered $MoSe_2$ nanosheets. The decomposition temperature of $MoSe_2$ (~650 °C) was reached after the CVD growth for 10 min, which is supposed to induce Se vacancies in $MoSe_2$. Such defects are believed to be the origin of the observed ambipolar conduction in our multilayer $MoSe_2$ TFTs, through the Fermi level pinning at the metal-$MoSe_2$ semiconductor interface. Moreover, the Se vacancies can enhance the optical properties of $MoSe_2$ devices, which were manifested by the highest photoresponsivity (93.7 A/W) reported to date and a fast response time ($\tau_{rise} \sim 0.4$ s) to the incident light. The results presented in this work will open up a new route for the fabrication of interactive electronics incorporating active-matrix displays and photosensing devices.

Methods

Synthesis of hexagonal $MoSe_2$ particles. $MoSe_2$ films were synthesized inside a CVD furnace composed of two zones; a 2-inch diameter horizontal tube furnace with a 2-inch diameter quartz tube. MoO_3 powders (Sigma Aldrich 99.5% purity) were placed on the right side of an alumina boat. Se powders (Sigma Aldrich 99.5% purity) were placed on the left side of the same boat. A 3 × 3 cm Si wafer with 300 nm SiO_2 grown on it was cleaned using acetone and isopropyl alcohol. The substrate was placed on top of the boat that is facing up. This configuration positions the sources in the hot zone and the substrate in the cold zone. The hot and cold zones were heated up to 800 °C and 750 °C, respectively, at 15 °C/min. The reaction chamber was constantly filled with 120 sccm Ar and 20 sccm H_2 gas for 20 min to allow the reaction to take place. After $MoSe_2$ growth for 20 min, the chamber was slowly cooled down to 650 °C for 10 min to generate Se vacancies and quenched to room temperature.

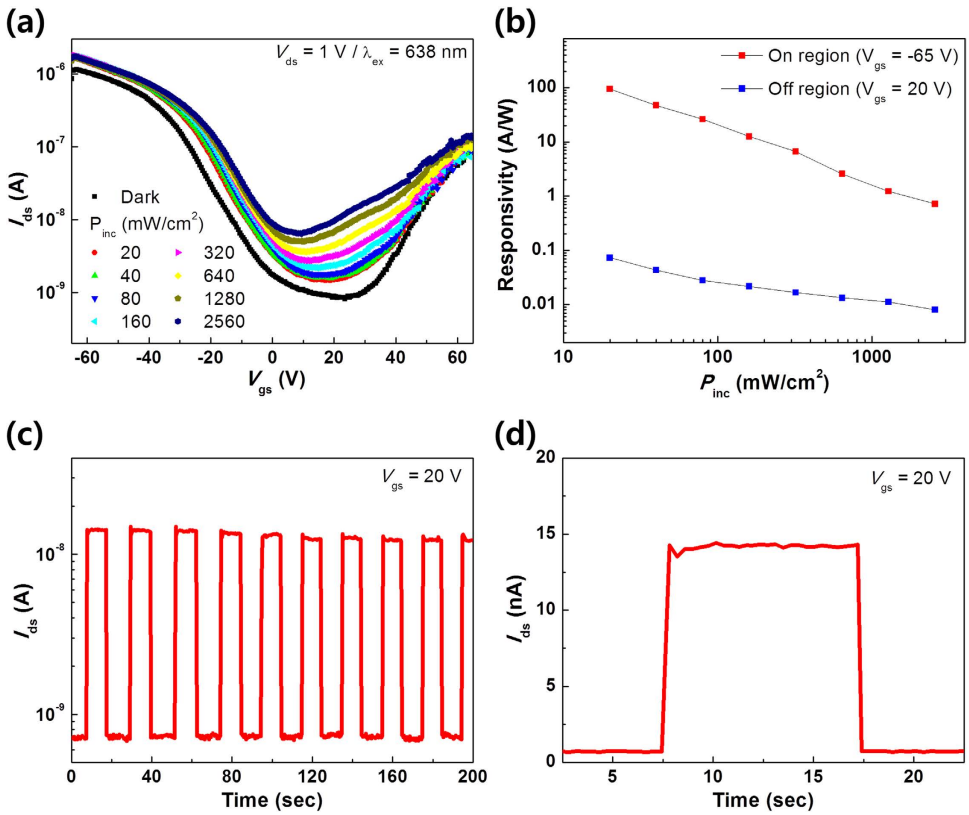

Figure 5. Photoresponsive behavior of hexagonal $MoSe_2$ TFT. (**a**) Comparison of transfer characteristics ($I_{ds} - V_{gs}$) in the dark and under illumination with different optical power densities ($\lambda_{ex} = 638$ nm, $P_{inc} = 20$, 40, 80, 160, 320, 640, 1280 and 2560 mW/cm^2). (**b**) Responsivity of the device in logarithmic scale in the on ($V_{gs} = -65$ V) and off ($V_{gs} = 20$ V) regions. (**c**) Switching behavior (I_{ds} – Time) of the photodetector at $V_{gs} = 20$ V. The device was switched on and off with the laser ($\lambda_{ex} = 638$ nm) at an interval of 10 s (a period of 20 s). (**d**) One cycle of the laser pulse, showing the drain current in the off region at $V_{gs} = 20$ V on a linear-scale of (**c**).

Synthesis of triangular bilayer $MoSe_2$ particles. The substrate and sources were put on the same place of the multilayer growth method. The critical differences between the two growth methods were injection gas quantity and the chamber pressure. The chamber was created a vacuum state using a pump. After purging, the gases, 50 sccm Ar and 10 sccm H_2, were constantly injected in the reaction chamber during the growth process. The reaction chamber pressure was kept around the atmospheric pressure. The other processes were same as the multilayer growth method.

Device fabrication. For the source and drain electrode, Ti (20 nm) was first deposited as an adhesion layer and Au was then grown (300 nm) using e-beam evaporation at room temperature. The electrodes were patterned by photolithography, resulting in a channel length of 6.35 μm. The as-fabricated device was annealed at 200 °C under atmospheric conditions for 2 h while being exposed to 100 sccm Ar and 10 sccm H_2 gas to eliminate the photoresist residue and to reduce the contact resistance.

Characterization. Optical images of the hexagonal $MoSe_2$ TFT were taken using an optical microscope (BX51M, Olympus Co., JAPAN) with white light (100 W halogen lamp, U-LH100-3) in bright field imaging mode and a 50× objective lens. The TEM images and diffraction patterns were obtained using a transmission electron microscope (FEI Tecnai^{TM} F20) operated at an acceleration voltage of 200 kV. For TEM sample preparation, the sample was cut to a 3 mm disk and the backside of the sample was hand-polished and dimpled down to about 5–10 μm at the center of the sample. Then, the sample was ion-milled from the backsides at a 4.5° angle and at 4.5 kV using a Gatan PIPS^{TM} until the small hole at the center of the sample was made. The topography of the $MoSe_2$ phototransistor was measured using an AFM (XE7 Atomic Force Microscope, Park Systems, South Korea) under non-contact mode with a 0.2 Hz scan rate. The electrical characteristics of the phototransistor were measured using a parameter analyzer (Keithley 4200 SCS) at room temperature. The photoresponsive properties of the $MoSe_2$ phtotransistor were evaluated using an illumination system composed of a Nikon Ti-e microscope with an Acton SP2300 spectroscope and a Zolix TLS3900x-500 tunable light source.

References

1. Ahn, S. E. *et al.* Metal oxide thin film phototransistor for remote touch interactive displays. *Adv. Mater.* **24,** 2631–2636 (2012).
2. Lee, Y. H. *et al.* Synthesis of Large-Area MoS_2 Atomic Layers with Chemical Vapor Deposition. *Adv. Mater.* **24,** 2320–2325 (2012).
3. Jeon, J. *et al.* Layer-controlled CVD growth of large-area two-dimensional MoS_2 films. *Nanoscale* **7,** 1688–1695 (2015).
4. Schmidt, H. *et al.* Transport properties of monolayer MoS_2 grown by chemical vapor deposition. *Nano Lett.* **14,** 1909–1913 (2014).
5. Lee, Y.-H. *et al.* Synthesis and transfer of single-layer transition metal disulfides on diverse surfaces. *Nano Lett.* **13,** 1852–1857 (2013).
6. Choi, W. *et al.* High-detectivity multilayer MoS_2 phototransistors with spectral response from ultraviolet to infrared. *Adv. Mater.* **24,** 5832–5836 (2012).
7. Roy, T. *et al.* Field-effect transistors built from all two-dimensional material components. *ACS Nano* **8,** 6259–6264 (2014).
8. Kim, S. *et al.* High-mobility and low-power thin-film transistors based on multilayer MoS_2 crystals. *Nat. Commun.* **3,** 1011 (2012).
9. Kwon, J. *et al.* Giant Photoamplification in Indirect-Bandgap Multilayer MoS_2 Phototransistors with Local Bottom-Gate Structures. *Adv. Mater.* **27,** 2224–2230 (2015).
10. Tongay, S. *et al.* Thermally driven crossover from indirect toward direct bandgap in 2D semiconductors: $MoSe_2$ versus MoS_2. *Nano Lett.* **12,** 5576–5580 (2012).
11. Kong, D. *et al.* Synthesis of MoS_2 and $MoSe_2$ films with vertically aligned layers. *Nano Lett.* **13,** 1341–1347 (2013).
12. Huang, J.-K. *et al.* Large-area synthesis of highly crystalline WSe_2 monolayers and device applications. *ACS Nano* **8,** 923–930 (2013).
13. Zhang, W. *et al.* Role of Metal Contacts in High-Performance Phototransistors Based on WSe_2 Monolayers. *ACS Nano* **8,** 8653–8661 (2014).
14. Ly, T. H. *et al.* Observing Grain Boundaries in CVD-Grown Monolayer Transition Metal Dichalcogenides. *ACS Nano* **8,** 11401–11408 (2014).
15. Liu, K.-K. *et al.* Growth of large-area and highly crystalline MoS_2 thin layers on insulating substrates. *Nano Lett.* **12,** 1538–1544 (2012).
16. Utama, M. I. B., Lu, X., Yuan, Y. & Xiong, Q. Detrimental influence of catalyst seeding on the device properties of CVD-grown 2D layered materials: A case study on $MoSe_2$. *Appl. Phys. Lett.* **105,** 253102 (2014).
17. Shim, G. W. *et al.* Large-area single-layer $MoSe_2$ and its van der Waals heterostructures. *ACS Nano* **8,** 6655–6662 (2014).
18. Shaw, J. C. *et al.* Chemical vapor deposition growth of monolayer $MoSe_2$ nanosheets. *Nano Res.* **7,** 511–517 (2014).
19. Lu, X. *et al.* Large-area synthesis of monolayer and few-layer $MoSe_2$ films on SiO_2 substrates. *Nano Lett.* **14,** 2419–2425 (2014).
20. Chang, Y.-H. *et al.* Monolayer $MoSe_2$ grown by chemical vapor deposition for fast photodetection. *ACS Nano* **8,** 8582–8590 (2014).
21. Helveg, S. *et al.* Atomic-scale structure of single-layer MoS_2 nanoclusters. *Phys. Rev. Lett.* **84,** 951 (2000).
22. Hirth, J. P. & Pound, G. M. *Condensation and evaporation; nucleation and growth kinetics*. (Macmillan, 1963).
23. Libera, J. & Gogotsi, Y. Hydrothermal synthesis of graphite tubes using Ni catalyst. *Carbon* **39,** 1307–1318 (2001).
24. Reina, A. *et al.* Large area, few-layer graphene films on arbitrary substrates by chemical vapor deposition. *Nano Lett.* **9,** 30–35 (2008).
25. Larentis, S., Fallahazad, B. & Tutuc, E. Field-effect transistors and intrinsic mobility in ultra-thin $MoSe_2$ layers. *Appl. Phys. Lett.* **101,** 223104 (2012).
26. Utama, M. I. B. *et al.* Etching-free patterning method for electrical characterization of atomically thin $MoSe_2$ films grown by chemical vapor deposition. *Nanoscale* **6,** 12376–12382 (2014).
27. Lee, L. T. L. *et al.* Few-layer $MoSe_2$ possessing high catalytic activity towards iodide/tri-iodide redox shuttles. *Sci. Rep.* **4,** 4063 (2014).
28. Wang, X. *et al.* Chemical vapor deposition growth of crystalline monolayer $MoSe_2$. *ACS Nano* **8,** 5125–5131 (2014).
29. Tongay, S. *et al.* Defects activated photoluminescence in two-dimensional semiconductors: interplay between bound, charged, and free excitons. *Sci. Rep.* **3,** 2657 (2013).
30. Das, S., Chen, H. Y., Penumatcha, A. V. & Appenzeller, J. High performance multilayer MoS_2 transistors with scandium contacts. *Nano Lett.* **13,** 100–105 (2012).
31. McDonnell, S. *et al.* Defect-Dominated Doping and Contact Resistance in MoS_2. *ACS Nano.* **8,** 2880–288 (2014).
32. Chen, C., Abe, K., Kumomi, H. & Kanicki, J. Density of states of a-InGaZnO from temperature-dependent field-effect studies. *IEEE Trans. Electron Devices* **56,** 1177–1183 (2009).
33. Lee, Y., Lee, J., Kim, S. & Park, H. S. Rendering high charge density of states in ionic liquid-gated MoS_2 transistors. *J. Phys. Chem. C* **118,** 18278–18282 (2014).
34. Yun, W. S., Han, S., Hong, S. C., Kim, I. G. & Lee, J. Thickness and strain effects on electronic structures of transition metal dichalcogenides: 2H-MX_2 semiconductors (M=Mo, W; X=S, Se, Te). *Phys. Rev. B* **85,** 033305 (2012).
35. Scheer, R. & Schock, H.-W. *Chalcogenide Photovoltaics: Physics, Technologies, and Thin Film Devices*. (John Wiley & Sons, 2011).
36. Bardeen, J. Surface states and Rectification at a Metal Semi-conductor Contact. *Phys Rev.* **71,** 717 (1947).
37. Xia, J. *et al.* CVD synthesis of large-area, highly crystalline $MoSe_2$ atomic layers on diverse substrates and application to photodetectors. *Nanoscale* **6,** 8949–8955 (2014).
38. Abderrahmane, A. *et al.* High photosensitivity few-layered $MoSe_2$ back-gated field-effect phototransistors. *Nanotechnology* **25,** 365202 (2014).
39. Fan, C. *et al.* Low temperature electrical and photo-responsive properties of $MoSe_2$. *Appl. Phys. Lett.* **104,** 202105 (2014).
40. Lopez-Sanchez, O., Lembke, D., Kayci, M., Radenovic, A. & Kis, A. Ultrasensitive photodetectors based on monolayer MoS_2. *Nat. Nanotechnol.* **8,** 497–501 (2013).

Acknowledgements

This research was supported in part by the National Research Foundation of Korea (NRF-2013M3C1A3059590, NRF-2014M3A9D7070732) and NSERC Discovery Grant (RGPIN-05920-2014). This work was also supported in part by the Korea Institute of Science and Technology (KIST) Institutional Program (Project No. 2Z04470). G.H. acknowledges the financial support by NSERC Canada Graduate Scholarships Program and WIN Nanofellowship.

Author Contributions

S.K. and J.P. designed the experiments. C.J., H.M., Y.K.H., J.P. and S.K. synthesized $MoSe_2$ film and fabricated the devices, and S.M.K., J.K. and I.O. characterized the quality of $MoSe_2$ film, and G.H. and Y.Y. planned the theoretical analysis. S.K., C.J., S.M.K., Y.Y. and J.P. wrote the manuscript. All authors reviewed the manuscript. C.J., H.M. and S.M.K. contributed equally to this work.

Additional Information

Competing financial interests: The authors declare no competing financial interests.

How to cite this article: Jung, C. *et al.* Highly Crystalline CVD-grown Multilayer $MoSe_2$ Thin Film Transistor for Fast Photodetector. *Sci. Rep.* **5**, 15313; doi: 10.1038/srep15313 (2015).